Ramsey interferometry for resonant Auger decay through core-excited states

Souvik Chatterjee and Takashi Nakajima*
Institute of Advanced Energy, Kyoto University, Gokasho, Uji, Kyoto 611-0011, Japan
(Received 11 March 2016; published 24 August 2016)

We theoretically investigate the electron dynamics in Ne atoms involving core-excited states through the Ramsey scheme with a pair of time-delayed x-ray pulses. Irradiation of Ne atoms by the ∼1 femtosecond x-ray pulse simultaneously populates two core-excited states, and an identical but time-delayed x-ray pulse probes the dynamics of the core-excited electron wave packet which is subject to the resonant Auger decay. The energy-integrated total Auger electron yield and energy-resolved Auger electron spectra in the time domain show periodic structures due to the temporal evolution of the wave packet, from which we can obtain the counterpart in the frequency domain through the Fourier transformation. The Auger electron energy spectra in the time as well as frequency domains show the interference patterns between the two Auger electron wave packets released into the continuum from the superposition of two core-excited states at different times. These spectra are important to clarify the individual contribution of the different Auger decay channels upon core excitation by the x-ray pulse.

DOI: 10.1103/PhysRevA.94.023417

I. INTRODUCTION

Recent advancements in the attosecond x-ray and XUV pulse technology have opened widespread opportunities for the real-time probing of ultrafast processes such as autoionization and Auger decay. Establishing a method to probe those processes has an undoubted scientific importance, since they originate from one of the most important interactions in physics and chemistry, i.e., electron-electron correlations. However, the x-ray pump–x-ray probe experiment is still at its early stage, since the attosecond XUV pulses generated by the high-harmonic processes have very limited intensity, while x-ray free electron lasers (FELs), which have sufficient intensity, suffer from the lack of temporal coherence. As a result, the popular probing method that is currently in use is the x-ray pump-infrared (IR) probe scheme in which the electron dynamics triggered by the x-ray pump pulse is probed by the time-delayed IR probe pulse. Such a method was successfully applied for the direct tracing of Auger electron dynamics with attosecond time resolution, and the lifetime of the core-excited state was accurately estimated [1]. Following the pioneering work [1], several different experiments were performed for the time-resolved probe of autoionization processes [2–6]. Note that the use of an IR pulse as a probe causes undesired and unavoidable complications if the purpose is to study the electron dynamics induced solely by the x-ray pump pulse.

Obviously, the use of an x-ray pump–x-ray probe scheme would be more effective in probing the x-ray-induced ultrafast processes, since there is no additional complication since the intense IR pulse is absent. Among the various kinds of pump-probe schemes the Ramsey interferometric scheme [7] is a very powerful method applicable to a variety of processes such as bound-free transitions [8], autoionization [9], and normal Auger process [10]. In the time-domain Ramsey scheme a pair of time-delayed identical pulses induces interference between the time-delayed bound and/or free electron wave packets launched at different times in atoms and molecules. The interference pattern of the signal obtained as a function of time delay between the two pulses are termed as Ramsey fringes. An important advantage of the Ramsey interferometric scheme is that it is highly effective even at low laser intensity, and therefore, can be implemented with attosecond pulses at modest intensities. Recently, XUV pump–XUV probe studies were experimentally performed to probe the electron dynamics in atoms with a time resolution of ∼1 femtosecond [11,12].

The purpose of this work is to theoretically investigate the dynamics of resonant Auger (RA) processes by the x-ray pump–x-ray probe Ramsey interferometry scheme. Since the employed x-ray pulses are necessarily short and hence spectrally broad, it is natural to assume that the x-ray pulse excites more than one core-excited state from which the RA decay occurs. Different from the normal Auger process, the RA process is initiated by the resonant excitation of core-excited state(s), and it is classified into the Auger spectator and Auger participator processes [13], and the recent advent of x-ray FELs has opened opportunities to study various aspects of RA processes [14–19]. Such a fundamental interferometric scheme allows a high-precision measurement of the position of the RA lines. Moreover, the strong dependence of the Ramsey fringes on the quantum coherence of the system facilitates the probing of coherence and measurement of decoherence time [10], in the case of RA processes. The x-ray Ramsey interferometric scheme can also be implemented for the measurement of any field induced Stark shifts [20–22].

II. THEORY

A. Model

Figure 1 shows the scheme we study. An x-ray pump pulse with ∼1-fs duration excites Ne atoms in the ground state, $|g\rangle$ ($1s^2 2s^2 2p^6$ at 0 eV), to two core-excited states, $|a_1\rangle$ ($1s^{-1}3p$ at 867.1 eV) and $|a_2\rangle$ ($1s^{-1}4p$ at 868.7 eV), respectively. The core-excited states decay into the continuum states, $|f_1,\varepsilon_1\rangle$ (Ne^+ $2p^4 3p$ at 55.8 eV + free electron) and $|f_2,\varepsilon_2\rangle$ (Ne^+ $2p^4 4p$ at 59.8 eV + free electron), through the RA process within the time scale of a few fs, as a result of which Auger electrons are produced. Here f_k ($k = 1,2$) represents the ionic states of Ne^+ which are formed upon the RA decay

*nakajima@iae.kyoto-u.ac.jp

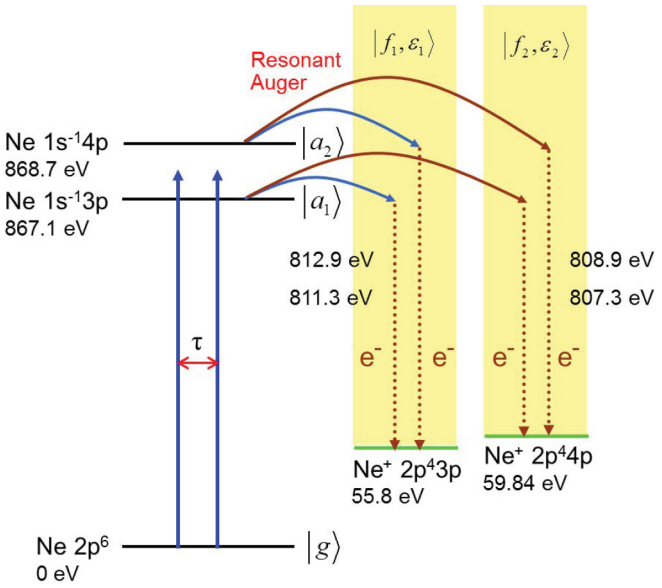

FIG. 1. Level scheme. A resonant x-ray pump pulse couples the ground state $|g\rangle$ to two core-excited states, $|a_1\rangle$ ($1s^{-1}3p$) and $|a_2\rangle$ ($1s^{-1}4p$), simultaneously. After the core excitation the RA decay into the continuum states, $|f_1,\varepsilon_1\rangle$ ($Ne^+\ 2p^4 3p$ + free electron) and $|f_2,\varepsilon_2\rangle$ ($Ne^+\ 2p^4 4p$ + free electron), takes place. The electron dynamics after the pump pulse is probed by the identical x-ray probe pulse with a variable time delay.

from states $|a_1\rangle$ and $|a_2\rangle$, respectively, while ε_k ($k = 1,2$) is the energy of free electrons emitted into the continuum. The channels where the core-excited electrons remain unchanged, $1s^{-1}3p$-$2p^4 3p$ and $1s^{-1}4p$-$2p^4 4p$, are usually the dominant channels, since they involve two electron Coulomb decay matrix elements. The two cross channels, $1s^{-1}3p$-$2p^4 4p$ and $1s^{-1}4p$-$2p^4 3p$ involving three electron matrix elements, described as shake up or down spectator decays, are less probable. Since we are using relatively weak pulse the x-ray induced direct photoionization from the ground state will be negligible and hence have been neglected in our model. The dynamics induced by the pump pulse are probed by the time-delayed identical probe pulse. This is a so-called Ramsey scheme in the time domain at the x-ray wavelength with two core-excited states as upper states. As mentioned above, the use of a resonant x-ray pump pulse with very short duration can excite more than one core-excited state, and as a prototypical example, we assume two core-excited states as upper states.

Theoretical calculations of the above RA processes subject to the resonant x-ray pump and probe pulses are based on the solution of the time-dependent Schrödinger equation for the Ne atom.

The total time-dependent wave function, $\Psi(t)$, of the system shown in Fig. 1 can be expanded as

$$\Psi(t) = c_g(t)|g\rangle + e^{-i\omega t}\left[c_{a_1}(t)|a_1\rangle + c_{a_2}(t)|a_2\rangle\right] + \int e^{-i\omega t} c_{f_1}(\varepsilon_1,t)|f_1,\varepsilon_1\rangle d\varepsilon_1 + \int e^{-i\omega t} c_{f_2}(\varepsilon_2,t)|f_2,\varepsilon_2\rangle d\varepsilon_2, \quad (1)$$

where ω is the central frequency of the x-ray pump and probe pulses, and $c_m(t)$ ($m = g,a_1,a_2$) and $c_{f_k}(t)$ ($k = 1,2$) denote the time-dependent amplitudes of the states indicated by the subscripts. After the standard procedure which includes the rotating-wave approximation we arrive at the following set of coupled differential equations. It reads

$$i\dot{c}_g(t) = E_g c_g(t) + \sum_{i=1,2} D_{a_i g}{}^{\dagger} c_{a_i}(t), \quad (2)$$

$$i\dot{c}_{a_1}(t) = \left[E_{a_1} - \omega - \frac{i}{2}\Gamma_{a_1}\right] c_{a_1}(t) + D_{a_1 g} c_g(t) - i\pi\left[\sum_{j=1,2} V_{f_j a_1} V_{f_j a_2}\right] c_{a_2}(t), \quad (3)$$

$$i\dot{c}_{a_2}(t) = \left[E_{a_2} - \omega - \frac{i}{2}\Gamma_{a_2}\right] c_{a_2}(t) + D_{a_2 g} c_g(t) - i\pi\left[\sum_{j=1,2} V_{f_j a_2} V_{f_j a_1}\right] c_{a_1}(t), \quad (4)$$

$$i\dot{c}_{f_j}(\varepsilon_j,t) = \left[E_{f_j} + \varepsilon_j - \omega\right] c_{f_j}(\varepsilon_j,t) + V_{f_j a_1} c_{a_1}(t) + V_{f_j a_2} c_{a_2}(t). \quad (5)$$

In the above equations E_m are the energies of neutral atomic states $|m\rangle$ ($m = g,a_1,a_2$), while E_{f_j} ($j = 1,2$) are the energies of ionic states after the RA decay. Γ_k are the total Auger decay rates of states $|k\rangle$ ($k = a_1,a_2$). $V_{f_j a_i}$ are the Coulomb matrix elements between the core-excited states, $|a_i\rangle$ ($i = 1,2$), and the associated continuum states, $|f_j,\varepsilon_j\rangle$ ($j = 1,2$), coupled by the RA decay, and they are connected to the partial Auger decay rates, $\Gamma_{f_j}^{(a_i)}$, through the relation of [23,24]

$$\Gamma_{f_j}^{(a_i)}(\varepsilon_j) = 2\pi\left|V_{f_j a_i}(\varepsilon_j)\right|^2. \quad (6)$$

The Coulomb matrix elements $V_{f_j a_i}$ would vary slowly with ε_k ($k = 1,2$) [13], because the kinetic energy of the Auger electrons is high. As a result, we can safely assume that $V_{f_j a_i}$ is practically constant over the continuum energies ε_j of interest. $D_{a_i g}$ ($i = 1,2$) are the Rabi frequencies between states $|a_i\rangle$ and $|g\rangle$, and they are expressed as

$$D_{a_i g} = \tfrac{1}{2}\mu_{a_i g} E(t), \quad (7)$$

where $\mu_{a_i g}$ ($i = 1,2$) are the dipole matrix elements between states $|g\rangle$ and $|a_i\rangle (i = 1,2)$. Finally, $E(t)$ is a field amplitude of the x-ray pump and probe pulses, and we assume that both pulses have Gaussian temporal profiles with time delay τ. Namely,

$$E(t) = E_0 \exp\left[-4\ln 2\left(\frac{t}{\sigma}\right)^2\right] + E_0 \exp\left[-4\ln 2\left(\frac{t-\tau}{\sigma}\right)^2\right], \quad (8)$$

where σ is the duration of x-ray pulses defined by the full width at half maximum (FWHM) for the field envelope. E_0 is the peak field amplitude of the x-ray pulse, which is assumed to be the same for both pump and probe pulses. The total Auger electron yield $P_{\rm tot}$, calculated after a sufficiently long time after

the probe pulse to allow complete decay of the core-excited states into the continuum, can be calculated using

$$P_{\rm tot}(\tau) = 1 - \lim_{t\to\infty} |c_g(t,\tau)|^2, \tag{9}$$

while the Auger electron energy spectra $P(\varepsilon_j,\tau)$, into the two continuum states $|f_j,\varepsilon_j\rangle$ $(j = 1,2)$ through the RA decay by the pump and probe pulses with time delay τ can be calculated by

$$P(\varepsilon_j,\tau) = \lim_{t\to\infty} |c_{f_j}(\varepsilon_j,t,\tau)|^2. \tag{10}$$

B. Analytical expression for the Auger electron energy spectra

Under the weak excitation regime we can derive a simple analytic expression for the Auger electron energy spectra for the two time-delayed x-ray pulse scenarios. In our derivation we neglect the non-Hermitian terms involving the Coulomb matrix elements [last terms in Eqs. (3) and (4)] of the respective core-excited states, because these terms make almost negligible contributions. We formally integrate Eq. (5) to obtain

$$c_{f_j}(\varepsilon_j,t) = -i \sum_{i=1,2} V_{f_j a_i} \exp\big[-i\big(E_{f_j}+\varepsilon_j-\omega\big)t\big] \times \int_{-\infty}^{t} \exp\big[i\big(E_{f_j}+\varepsilon_j-\omega\big)t'\big] \sum_{i=1,2} c_{a_i}(t)dt'. \tag{11}$$

After invoking the RWA and recalling that $c_g \sim 1$ under a weak excitation regime, we obtain

$$P(\varepsilon_j,\tau) = \left| \sum_{i=1,2} \frac{V_{f_j a_i}\mu_{a_i g}}{E_{f_j}+\varepsilon_j - E_{a_i} - \frac{i}{2}\Gamma_{a_i}} \right|^2 \times \big|E\big(\tau, E_{f_j}+\varepsilon_j-\omega\big)\big|^2, \tag{12}$$

where $E(\tau, E_{f_j}+\varepsilon_j-\omega)$ is the spectral envelope of the time-delayed x-ray pulses expressed as

$$E\big(\tau,E_{f_j}+\varepsilon_j-\omega\big) = \frac{E_0\sigma}{\sqrt{8\ln 2}} \exp\left[-\big(E_{f_j}+\varepsilon_j-\omega\big)^2 \frac{\sigma^2}{16\ln 2}\right] \times \big\{\big[1+\exp\big[-i\big(E_{f_j}+\varepsilon_j-\omega\big)\tau\big]\big\}. \tag{13}$$

III. NUMERICAL RESULTS AND DISCUSSIONS

Before presenting the numerical results we state the important assumptions and specify the parameters employed for the numerical calculations. We perform the calculations using three different photon energies, 867.6, 867.9, and 868.7 eV, for the x-ray pulses. The peak intensity and the duration of the x-ray pulses for the field envelope are 10^{17} W/cm^2 and 1.2 fs, respectively, unless otherwise mentioned. The duration of the x-ray pulses for the intensity envelope is around 0.6 fs. Generation of such sub-fs x-ray pulses at the Ne-K edge should be feasible by selectively spoiling the transverse emittance of the electron beam and applying such a system to the Linac Coherent Light Source (LCLS) [25,26]. The use of such sub-fs x-ray pulses, due to their large spectral bandwidth, can excite several core-excited states simultaneously. However, the transition dipole moment from the ground state to the core-excited state, $1s^{-1}np$, becomes smaller as n increases. In our specific case, the dipole matrix elements for the Ne atom are $\mu_{a_1 g}$=0.0096 (a.u.) [18] and $\mu_{a_2 g}$=0.0059 (a.u.) [27], respectively, where $|a_1\rangle = 1s^{-1}3p$ and $|a_2\rangle = 1s^{-1}4p$. Together with the detuning consideration of x-ray pulses from resonances, we can say that the third state such as $1s^{-1}5p$ can be safely neglected to investigate the core excitation by sub-fs x-ray pulses. As additional information we note that the lifetimes of the core-excited states are ∼2.41 fs for both states, $|a_1\rangle$ and $|a_2\rangle$, and the Coulomb matrix elements $V_{f_j a_i}$ are calculated using the partial width values reported in [27].

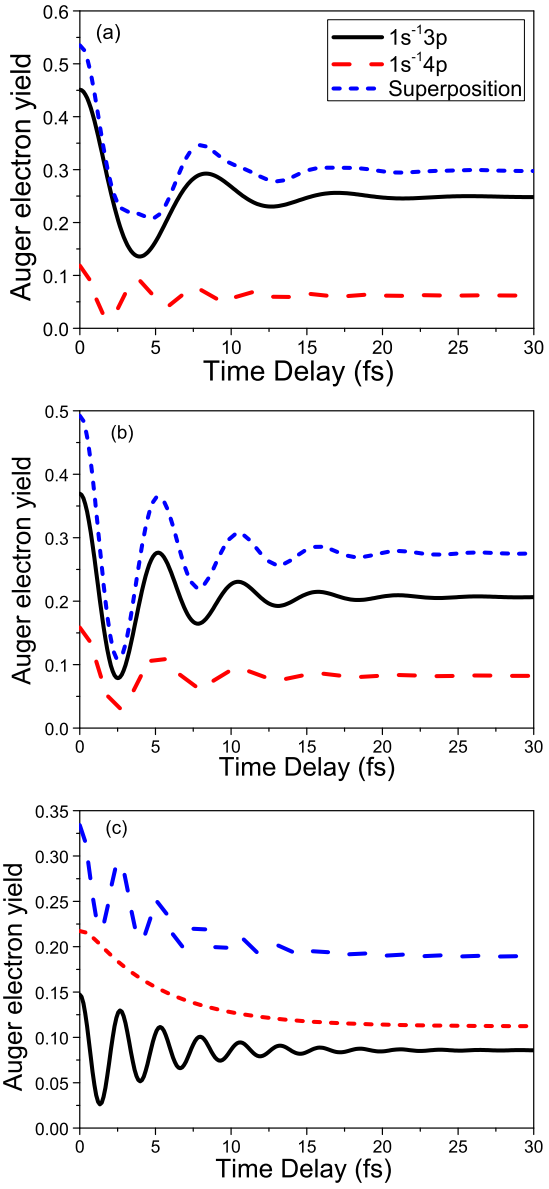

FIG. 2. Variation of the total Auger electron yield as a function of time delay between the pump and probe pulses. Employed photon energies are (a) 867.6, (b) 867.9, and (c) 868.7 eV, respectively.

Figure 2 shows the variation of the total Auger electron yields $P_{\rm tot}$ as a function of time delay between the pump and probe pulses at three different photon energies, 867.6, 867.9,

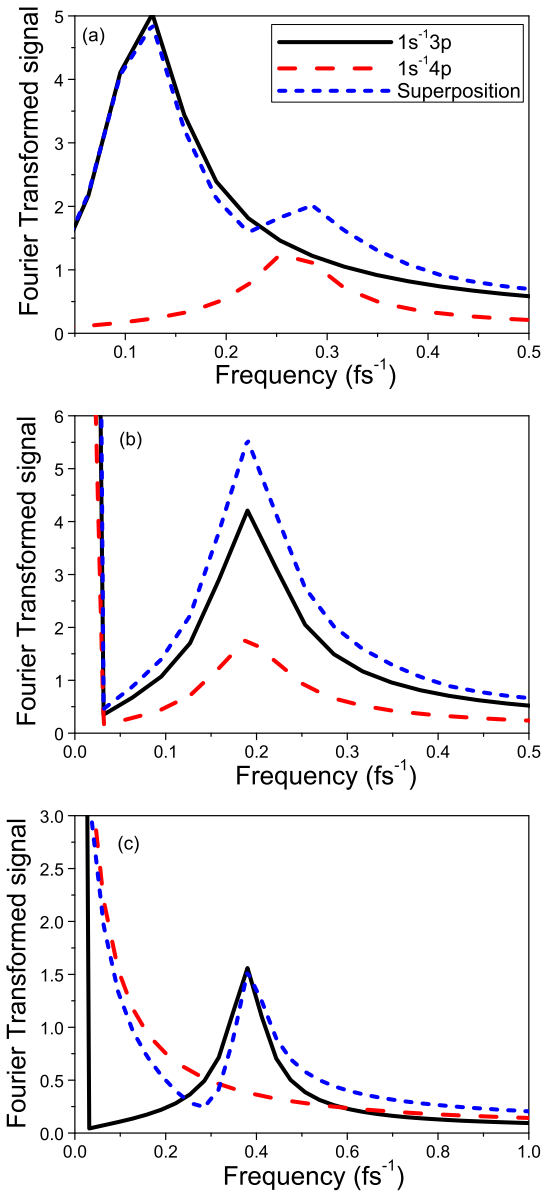

FIG. 3. Fourier transform of Fig. 2.

and 868.7 eV. In each panel of Figs. 2(a)– 2(c) we plot three curves for the three different computational conditions: The curves of "$1s^{-1}3p$" ("$1s^{-1}4p$") in Fig. 2 imply that only one core-excited state, $1s^{-1}3p$ ($1s^{-1}4p$), is assumed as an upper state, while the curve of "Superposition" implies that both core-excited states are assumed as upper states. Now we look into the detail of the results in Fig. 2. For the photon energy of 867.6 eV which is close to the transition frequency to $1s^{-1}3p$ from the ground state [Fig. 2(a)], the Auger electron yields exhibit modulations at the frequencies given by $|E_{a_1} - \omega|^{-1}$. Indeed, Fourier transform of Fig. 2(a), which is shown in Fig. 3(a), reveals two major frequency components corresponding to $|E_{a_1} - \omega|^{-1}$ and $|E_{a_2} - \omega|^{-1}$. At this photon energy, the Auger electron yield from state $1s^{-1}3p$ is much larger than that from state $1s^{-1}4p$, because the dipole moment from the ground state to the former state is much larger than that to the latter state. For the photon energy of 867.9 eV, falling midway between the two core-excited states, $E_{a_1} - \omega = E_{a_2} - \omega$, and accordingly the modulation frequencies of the three Auger electron yields are exactly the same [Figs. 2(b) and 3(b)]. Next we choose the photon energy of 868.7 eV, which is on resonance with state $1s^{-1}4p$ from the ground state [Fig. 2(c)]. For this case the Auger electron yield from state $1s^{-1}4p$ is appreciably increased, and becomes comparable to that from state $1s^{-1}3p$. Obviously, the Auger electron yield from $1s^{-1}4p$ does not show a modulation, since $E_{a_2} - \omega = 0$, while the modulation period of the Auger electron yield for the case of $1s^{-1}3p$ as an upper state [Fig. 2(c)] corresponds to the energy difference between $1s^{-1}3p$ and $1s^{-1}4p$, which we rediscover in Fig. 3(c). What we can learn from Figs. 2 and 3 is that the energy difference of the core-excited states, which lie very high in energy from the ground state, can be precisely obtained from the (energy-integrated) modulation period of the total Auger electron yield as a function of time delay between the pump and probe pulses.

The time-dependent dynamics of the (energy-integrated) total Auger electron yield and the corresponding results after Fourier transform shown above give us a much simplified picture, and any possible interference effect that originates from the release of Auger electron wave packets into the continuum from the superposition of two core-excited states at different times by the pump and probe pulses may have been smeared out. This would be particularly true if the period of modulation of the interference fringe in Auger electron energy spectra varies with the kinetic energies of the emitted Auger electrons. Moreover, the respective contributions of the different decay channels, considered in our theoretical model, to the overall Auger electron dynamics triggered by the x-ray pulses, cannot be determined from the delay-dependent variation of the total Auger electron yield we have shown in Fig. 2.

In order to obtain better understanding of the Auger electron dynamics we now look into the Auger electron energy spectra for different photon energies, 867.9 and 868.7 eV, as a function of time delay between the pump and probe pulses. For clarity we separately calculate the Auger electron energy spectra into the two continuum states, $P(\varepsilon_j,\tau)$ $(j = 1,2)$ associated with the ionic states, $2p^4 3p$ and $2p^4 4p$ (Fig. 1), respectively, and their Fourier transforms. The probability density of the Auger electron is represented in logarithmic scale in the Auger electron energy spectra and their Fourier transforms, respectively. The results for the photon energy of 867.9 eV are shown in Fig. 4 in which Figs. 4(a) and 4(b) are the Auger electron energy spectra into the two continua, $|f_1,\varepsilon_1\rangle$ (Ne^+ $2p^4 3p$ + free electron) and $|f_2,\varepsilon_2\rangle$ (Ne^+ $2p^4 4p$ + free electron), while Figs. 4(c) and 4(d) are the corresponding Fourier transforms. The Auger electron energy spectrum shown in Fig. 4(a) is dominated by the contribution coming from the RA processes from state $1s^{-1}3p$, and the contribution from the $1s^{-1}4p$ state, is much weaker, as mentioned earlier. A strong modulation with a period of 5.3 fs is visible at the electron energy of 811.3 and 807.3 eV in Figs. 4(a) and 4(b), respectively, which are the Auger electrons from state $1s^{-1}3p$. A much weaker modulation is visible for the Auger electrons at the energies of 812.9 and 808.9 eV emitted from the $1s^{-1}4p$ state. This is consistent with the results for the total Auger electron yields shown in Fig. 2(b), but more informative in

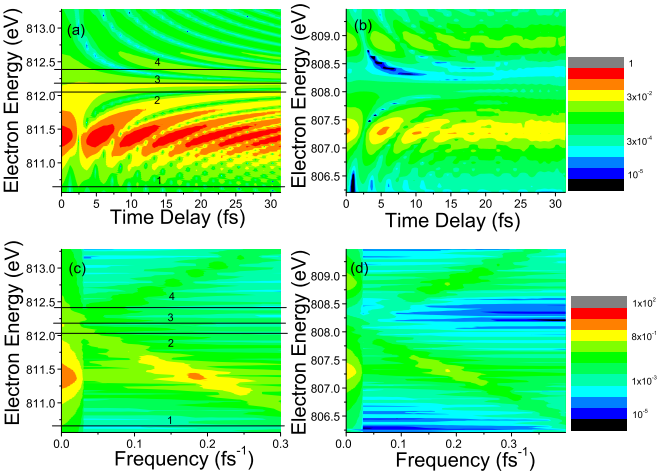

FIG. 4. Auger electron energy spectra as a function of time delay between the pump and probe pulses. Auger electron energy spectra into the continua associated with the ionic states of (a) $2p^4 3p$ and (b) $2p^4 4p$. Fourier transformed results of graphs (a) and (b) are presented in graphs (c) and (d), respectively. The photon energy is 867.9 eV.

a sense that the two well-separated beating patterns appear at energies that can be directly correlated to the $1s^{-1}3p$ and $1s^{-1}4p$ core-excited states, respectively. It may be noted that the peak at 812.9 eV is not so visible because the signal from the interference fringes around this energy region are comparatively stronger than that coming from the $1s^{-1}4p$ core excited state. The Fourier transformed results, Figs. 4(c) and 4(d), of Figs. 4(a) and 4(b), also show the consistency with Fig. 3(b).

The period of modulation for the Auger electron energies at 811.3 and 807.3 eV agrees well with the value of $|E_{a_1} - \omega|^{-1}$, and hence the well-resolved peaks in this energy region can be correlated to the $|a_1\rangle$ core-excited state. A similar pattern is found at the electron energies of 812.9 and 808.9 eV in Figs. 4(a) and 4(b), respectively, and the Fourier transformed counterparts, Figs. 4(c) and 4(d), which are associated with the Auger electrons from state $1s^{-1}4p$. However, the Auger electron density in these energy regions are very weak.

Interestingly, we can see a bending structure in the Auger electron energy spectra [Figs. 4(a) and 4(b)], which is similar to the one observed in the photoelectron spectra into the smooth continuum [8]. This is because the time-delayed pump and probe pulses launch the two electron wave packets, which interfere with each other, and the way they interfere is different, depending on not only the time delay but also on the electron energy. For a certain time delay τ, the energy spacing between the two adjacent fringes in the Auger electron energy spectra is given by $2\pi/\tau$ [8]. It is also interesting to note that the period of modulation observed in the Auger electron energy spectra [Figs. 4(a) and 4(b)] as a function of time delay is also dependent on the Auger electron energy. The origin of interference in the continuum and its dependence on time delay at a particular electron energy E can be understood from the simple expression, $(E + E_{f_j} - \omega)\tau = 2\pi n$, where n is an integer. Accordingly, the position of the interference fringes in the continuum, $E = \omega - E_{f_j} + (2\pi n/\tau)$, is determined.

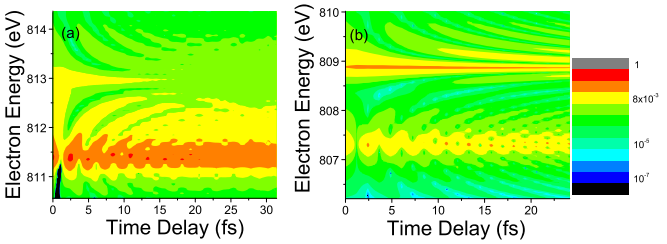

FIG. 5. Similar to Figs. 4(a) and 4(b) but calculated for the photon energy of 868.7 eV.

For a particular electron energy E, the modulation frequency of the interference fringes linearly varies with the electron energy according to the relation $(E + E_{f_j} - \omega)/2\pi n$. As a result, the modulation period increases as the Auger electron energy increases [line 1 → line 2 in Figs. 4(a) and 4(c)], and the modulation stops at the Auger electron energy of $E = \omega - E_{f_j}$ [lines 3 in Figs. 4(a) and 4(c)]. The periodic oscillation reappears with an inverted pattern for even higher Auger electron energies with the period of modulation showing a decreasing trend as the Auger electron energy is increased further [lines 4 in Figs. 4(a) and 4(c)]. All the above can be clearly seen in the Fourier transformed spectra where the two bending patterns merge to form a V-shaped structure [Fig. 4(c)]. Similar structures are also found in the Auger electron spectrum associated with the ionic state of $2p^4 4p$ [Fig. 4(b)] and its Fourier transform [Fig. 4(d)].

Similar calculations are performed for the photon energy of 868.7 eV, which is resonant with the ground–$1s^{-1}4p$ transition, and in Fig. 5 we present the Auger electron energy spectra as a function of time delay. Since the x-ray pulse resonantly excites state $1s^{-1}4p$ and hence $E_{a_2} - \omega = 0$, there occurs no modulation in the Auger electron energy spectrum at 808.9 eV which is associated with state $1s^{-1}4p$, while the modulation at 807.3 eV, associated with state $1s^{-1}3p$, is clearly seen. The trend of bending and inverted bending patterns observed at two different regions of Auger electron energy observed in Fig. 4 is also visible in the spectra displayed in Figs. 5(a) and 5(b). What we can see from the result shown in Figs. 4 and 5 is that the modulations which appear in the Auger electron energy spectra have two different origins. One is the modulation which originates from the temporal evolution of the core-excited state wave packet prior to its decay into the ionic continuum, and the other is the modulations which originate from the Ramsey interference.

For a better understanding of the involved physics in the time delay dependent Auger electron energy spectrum, we also compute the spectrum using the analytical expression shown in Eq. (13). The result is shown in Fig. 6. Note that the parameters employed for this computation are the same with those for Fig. 4(a) obtained by numerically solving Eqs. (1)– (5) together with Eqs. (8) and (10). It is evident from Fig. 6 that the analytical expression, which is simply a product of the stationary Auger electron spectrum and the squared modulus of the spectrum of the x-ray pulses, can reproduce the essential features of the numerically obtained spectra shown in Fig. 4(a). By inspecting the analytical expression we notice that the coherence of the x-ray pulses is imprinted on the resonant

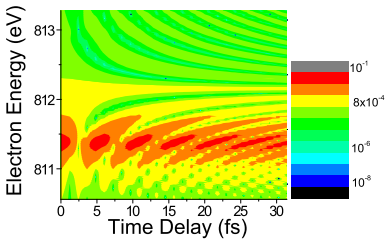

FIG. 6. Auger electron energy spectra as a function of time delay between the pump and probe pulses, similar to Fig. 4(a), calculated using analytical expression.

Auger electron dynamics of the core-excited state wave packet, which manifest themselves as interference patterns observed in the Auger electron energy spectrum as a function of time delay.

Needless to say, the contrast of Ramsey interference is maximum when the x-ray pulse is perfectly stable, as we have assumed so far. However, the currently available x-ray laser is a SASE-FEL type, from which the x-ray pulse is not very stable in terms of pulse spectrum. Therefore, it would be of practical interest to know how much interference survives for such fluctuating x-ray pulses. The numerical calculations of electron energy spectra with chaotic x-ray pulses are quite elaborative, and it is beyond the scope of the present work. Nevertheless, to obtain some insight, we employ a simple alternative approach: The x-ray pulses are still assumed to be transform limited with a Gaussian temporal envelope, but their central photon energies change from shot to shot by obeying the normal distribution function with a certain width for the central photon energy. The actual calculations are performed using the analytical expression [Eq. (12)] with the pulse parameters used for Figs. 4(a) and 6. The electron energy spectra obtained for x-ray pulses with different central photon energies are then averaged at each delay time after multiplying with appropriate weighting factors. The results are represented in Figs. 7(a) and 7(b) for the different widths of shot-to-shot photon energy fluctuations, which are 0.4 eV [Fig. 7(a)] and 0.2 eV [Fig. 7(b)], respectively, around the central photon energy of 867.9 eV. It is evident from Figs. 7(a) and 7(b) that the shot-to-shot fluctuation of the x-ray photon energy smears out the Ramsey interference fringes, as expected. It is to be noted that the beatings at around 811.4 eV due to temporal wave-packet evolution are

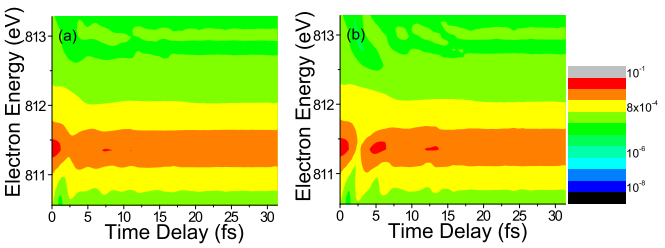

FIG. 7. Auger electron energy spectra, after averaging over different photon energy shots, as a function of time delay between the pump and probe pulses for a photon energy range of (a) 0.4 eV and (b) 0.2 eV, respectively. The pulse parameters are similar to Figs. 4(a) and 6.

visible in this Auger electron spectra. The feasibility for real time observation of any beating effect due to temporal wave-packet evolution on delay time variation, under the present x-ray facilities [28–31], has been stated in [32]. This further substantiates our findings. Moreover, the visibility of the beats and fringe pattern show significant improvements if the fluctuation range of central photon energy is narrowed 0.4–0.2 eV, as shown in Fig. 7(b). This gives a feeling of how precise the central photon energy has to be to observe the interference fringes.

IV. CONCLUSIONS

In this work we have theoretically investigated the electron dynamics in an atomic system involving two core-excited states through the time-domain Ramsey interferometry with a pair of x-ray pulses. Specific results have been presented for the Ne atom. We have found the periodic modulation in the (energy-integrated) total Auger electron yield as a function of time delay between the pump and probe pulses. The modulation simply arises from the temporal evolution of the core-excited state wave packet, and Fourier transform of the Auger electron yield as a function of time delay helps to clarify the origin of modulation. We have also studied the variation of Auger electron energy spectra as a function of time delay between the pump and probe pulses, and found the modulations, whose periods are different not only at different time delays but also at different electron energies. Importantly, there are two different origins of modulations, i.e., time evolution of the core-excited state wave packet and Ramsey interference, and only the modulation originating from the wave-packet evolution prior to Auger decay survives after the integration of the Auger electron signals over energy. The core-excited electron wave packets launched by the pump and probe pulses become the two Auger electron wave packets after the resonant Auger decay, and they interfere with each other in different ways at different electron energies, which results in the bending structure in the Auger electron energy spectra as a function of time delay, and these are essentially Ramsey fringes. The computed Auger electron spectra as a function of time delay show the periodic modulation in the region around 811.3 and 812.9 eV associated with the continuum belonging to the ionic state $2p^4 3p$, and also around 807.3 and 808.9 eV associated with the continuum belonging to ions in state $2p^4 4p$, respectively. This periodic modulation is a clear signature of the spatio-temporal evolution of the core-excited state wave packet before decaying into the continuum. Thus, we have shown that the Ramsey interferometric probing of atomic systems using a pair of time-delayed x-ray pulses is a powerful method to probe the detailed electron dynamics in a system subject to the resonant Auger decay.

ACKNOWLEDGMENTS

This work was supported by the Grant-in-Aid for scientific research from the Ministry of Education, Culture, Sports, Science and Technology (Japan).

[1] M. Drescher, M. Hentschel, R. Kienberger, M. Uiberacker, V. Yakovlev, A. Scrinzi, Th. Westerwalbesloh, U. Kleineberg, U. Heinzmann, and F. Krausz, Time-resolved atomic inner-shell spectroscopy, Nature (London) **419**, 803 (2002).

[2] M. Wickenhauser, J. Burgdörfer, F. Krausz, and M. Drescher, Time Resolved Fano Resonances, Phys. Rev. Lett. **94**, 023002 (2005).

[3] Z. X. Zhao and C. D. Lin, Theory of laser-assisted autoionization by attosecond light pulses, Phys. Rev. A **71**, 060702(R) (2005).

[4] S. Gilbertson, M. Chini, X. Feng, S. Khan, Y. Wu, and Z. Chang, Monitoring and Controlling the Electron Dynamics in Helium with Isolated Attosecond Pulses, Phys. Rev. Lett. **105**, 263003 (2010).

[5] H. Wang, M. Chini, S. Chen, C-H. Zhang, F. He, Y. Cheng, Y. Wu, U. Thumm, and Z. Chang, Attosecond Time-Resolved Autoionization of Argon, Phys. Rev. Lett. **105**, 143002 (2010).

[6] J. Mauritsson *et al.*, Attosecond Electron Spectroscopy Using a Novel Interferometric Pump-Probe Technique, Phys. Rev. Lett. **105**, 053001 (2010).

[7] N. F. Ramsey, The method of successive oscillatory fields, Phys. Today **33**, 25 (1980).

[8] M. Wollenhaupt, A. Assion, D. Liese, C. Sarpe-Tudoran, T. Baumert, S. Zamith, M. A. Bouchene, B. Girard, A. Flettner, U. Weichmann, and G. Gerber, Interferences of Ultrashort Free Electron Wave Packets, Phys. Rev. Lett. **89**, 173001 (2002).

[9] A. Pirri, E. Sali, C. Corsi, M. Bellini, S. Cavalieri, and R. Eramo, Extreme-ultraviolet Ramsey-type spectroscopy, Phys. Rev. A **78**, 043410 (2008).

[10] C. Buth and K. J. Schafer, Ramsey method for Auger-electron interference induced by an attosecond twin pulse, Phys. Rev. A **91**, 023419 (2015).

[11] E. Skantzakis, P. Tzallas, J. E. Kruse, C. Kalpouzos, O. Faucher, G. D. Tsakiris, and D. Charalambidis, Tracking Autoionizing-Wave-Packet Dynamics at the 1-fs Temporal Scale, Phys. Rev. Lett. **105**, 043902 (2010).

[12] P. Tzallas, E. Skantzakis, L. A. A. Nikolopoulos, G. D. Tsakiris, and D. Charalambidis, Extreme-ultraviolet pump-probe studies of one-femtosecond-scale electron dynamics, Nat. Phys. **7**, 781 (2011).

[13] G. B. Armen, H. Aksela, T. Åberg, and S. Aksela, The resonant Auger effect, J. Phys. B **33**, R49 (2000).

[14] N. Rohringer and R. Santra, Resonant Auger effect at high x-ray intensity, Phys. Rev. A **77**, 053404 (2008).

[15] J.-C. Liu, Y.-P. Sun, C.-K. Wang, H. Ågren, and F. Gel'mukhanov, Auger effect in the presence of strong x-ray pulses, Phys. Rev. A **81**, 043412 (2010).

[16] Y.-P. Sun, J.-C. Liu, C.-K. Wang, and F. Gel'mukhanov, Propagation of a strong x-ray pulse: Pulse compression, stimulated Raman scattering, amplified spontaneous emission, lasing without inversion, and four-wave mixing, Phys. Rev. A **81**, 013812 (2010).

[17] Ph. V. Demekhin and L. S. Cederbaum, Strong interference effects in the resonant Auger decay of atoms induced by intense x-ray fields, Phys. Rev. A **83**, 023422 (2011).

[18] A. Picón, C. Buth, G. Doumy, B. Krässig, L. Young, and S. H. Southworth, Optical control of resonant Auger processes, Phys. Rev. A **87**, 013432 (2013).

[19] S. Chatterjee and T. Nakajima, Manipulation of resonant Auger processes using a strong bichromatic field, Phys. Rev. A **91**, 043413 (2015).

[20] H. Häffner, S. Gulde, M. Riebe, G. Lancaster, C. Becher, J. Eschner, F. Schmidt-Kaler, and R. Blatt, Precision Measurement and Compensation of Optical Stark Shifts for an Ion-Trap Quantum Processor, Phys. Rev. Lett. **90**, 143602 (2003).

[21] V. I. Yudin, A. V. Taichenachev, C. W. Oates,. Z. W. Barber, N. D. Lemke, A. D. Ludlow U. Sterr, Ch. Lisdat, and F. Riehle, Hyper-Ramsey spectroscopy of optical clock transitions, Phys. Rev. A **82**, 011804(R) (2010).

[22] N. Huntemann, B. Lipphardt, M. Okhapkin, Chr. Tamm, E. Peik, A. V. Taichenachev, and V. I. Yudin, Generalized Ramsey Excitation Scheme with Suppressed Light Shift, Phys. Rev. Lett. **109**, 213002 (2012).

[23] V. F. Weisskopf and E. P. Wigner, Z. Phys. **63**, 54 (1930).

[24] R. Santra and L. S. Cederbaum, Non-Hermitian electronic theory and applications to clusters, Phys. Rep. **368**, 1 (2002).

[25] P. Emma, K. Bane, M. Cornacchia, Z. Huang, H. Schlarb, G. Stupakov, and D. Walz, Femtosecond and Subfemtosecond X-Ray Pulses from a Self-Amplified Spontaneous-Emission-Based Free-Electron Laser, Phys. Rev. Lett. **92**, 074801 (2004).

[26] Y. Ding *et al.*, Generating femtosecond X-ray pulses using an emittance-spoiling foil in free-electron lasers, Appl. Phys. Lett. **107**, 191104 (2015).

[27] N. Saito, N. M. Kabachnik, Y. Shimizu, H. Yoshida, H. Ohashi, Y. Tamenori, I. H. Suzuki, and K. Ueda, Interference effects in the branching ratio for the partial decay channels of the Ne $(1s^{-1}3p)$ resonance, J. Phys. B **33**, L729 (2000).

[28] A. A. Lutman, R. Coffee, Y. Ding, Z. Huang, J. Krzywinski, T. Maxwell, M. Messerschmidt, and H.-D. Nuhn, Experimental Demonstration of Femtosecond Two-Color X-Ray Free-Electron Lasers, Phys. Rev. Lett. **110**, 134801 (2013).

[29] E. Allaria *et al.*, Two-colour pump–probe experiments with a twin-pulse-seed extreme ultraviolet free-electron laser, Nat. Commun. **4**, 2476 (2013).

[30] A. Marinelli *et al.* High-intensity double-pulse X-ray free-electron laser, Nat. Commun. **6**, 6369 (2015).

[31] N. Hartmann *et al.*, Sub-femtosecond precision measurement of relative X-ray arrival time for free-electron lasers, Nat. Photon. **8**, 706 (2014).

[32] S. B. Zhang and N. Rohringer, Quantum-beat Auger spectroscopy, Phys. Rev. A **92**, 043420 (2015).